COMMUNICATIONS CHEMISTRY

ARTICLE

https://doi.org/10.1038/s42004-019-0194-4 OPEN

Design strategy for germanium-rhodamine based pH-activatable near-infrared fluorescence probes suitable for biological applications

Yuichiro Koide[1,7], Ryosuke Kojima[2,3,7], Kenjiro Hanaoka[1], Koji Numasawa[1], Toru Komatsu[1], Tetsuo Nagano[4], Hisataka Kobayashi[5] & Yasuteru Urano[1,2,6]

Fluorescence probes that can detect pH are useful tools for biological research and clinical diagnosis. Here we report pH-activatable near-infrared fluorescence probes, based on hydroxymethyl germanium-rhodamine (HMGeR), that are suitable for a range of biological applications. The pK_a, the ratio of the fluorescent form in an acidic environment, and the absorption/emission wavelengths can all be conveniently optimized. The most promising probe, 2-HM IGeR, offers significant advantages over currently available near-infrared pH probes, notably high quantum efficiency, appropriate pK_a value for biological applications, and high photostability. Further, our molecular design strategy allows easy conjugation of the probes to biomolecules without loss of functionality. We illustrate the value of this strategy by developing probe-Herceptin® and probe-avidin conjugates to visualize pH change in cellular vesicles during endocytosis, and to visualize tumors in a mouse model, respectively. We believe 2-HM IGeR is currently among the best-in-class pH-activatable near-infrared probes for biological and medical research.

[1] Graduate School of Pharmaceutical Sciences, The University of Tokyo, 7-3-1 Hongo, Bunkyo-ku, Tokyo 113-0033, Japan. [2] Graduate School of Medicine, The University of Tokyo, 7-3-1 Hongo, Bunkyo-ku, Tokyo 113-0033, Japan. [3] PRESTO, Japan Science and Technology Agency, 4-1-8 Honcho, Kawaguchi, Saitama 332-0012, Japan. [4] Drug Discovery Initiative, The University of Tokyo, 7-3-1 Hongo, Bunkyo-ku, Tokyo 113-0033, Japan. [5] Molecular Imaging Program, Center for Cancer Research, National Cancer Institute, National Institutes of Health, Bethesda, MD 20892, USA. [6] CREST, AMED, Japan Agency for Medical Research and Development, 1-7-1 Otemachi, Chiyoda-ku, Tokyo 100-0004, Japan. [7] These authors contributed equally: Yuichiro Koide, Ryosuke Kojima. Correspondence and requests for materials should be addressed to Y.U. (email: uranokun@m.u-tokyo.ac.jp)

Fluorescence probes that can detect pH (pH probes) are useful tools for both biological research and diagnosis, offering high sensitivity, good spatial and temporal resolution, and ease of use. For example, they are widely used to study cellular processes such as endocytosis, phagocytosis, exocytosis, and so on, that are accompanied by dynamic pH changes inside vesicles, influencing the activity of various enzymes[1–4]. Further, activatable pH probes (OFF/ON type) in combination with antibodies can visualize cancers selectively in vivo[5–7]. Generally, pH probes with pK_a around 6 are thought to be appropriate for such applications, because intracellular pH changes are centered around this pH[5].

Many pH probes have been reported[8–10], and some are commercially available. However, most of them require excitation in the visible region; however, light in this wavelength range induces autofluorescence of biomolecules, and is easily absorbed and scattered by tissue or skin, resulting in a low signal-to-noise ratio and non-quantitative detection capability during in vivo imaging. One approach to minimize these problems is to develop fluorescence probes whose absorption and emission wavelengths are in the near-infrared (NIR) region[11–13], because the tissue penetration of light in this region is much greater than that of visible light. NIR pH probes are also particularly useful for multi-color imaging of biological processes in cellulo[14–16], enabling plural molecular activities to be monitored simultaneously.

Some NIR pH probes that can detect acidic environments have been reported. However, most of them are cyanine-based probes, which become highly fluorescent or change their fluorescence properties when an amino group within the fluorophore is protonated[17–22]. These probes have various drawbacks, including inappropriate pK_a to monitor intracellular pH, irreversibility of response to pH change, and instability to photoirradiation. A sophisticated series of NIR pH probes for precisely measuring intracellular pH was recently developed[23], but these probes required ratiometric measurement, which is not easy to apply for in vivo cancer imaging in the clinical setting.

Herein, we report a Ge-rhodamine-based, OFF/ON type, pH-activatable probe that offers significant advantages over other currently available probes for analyzing biological processes or diseases in which pH changes play an important role, especially when a high signal-to-noise ratio in the NIR region is required.

Results

Our strategy for designing the probe. We focused on spirocyclization of rhodamine dyes as the basis for the probe design. It is known that a nucleophilic functional group such as amide, hydroxymethyl, or thiomethyl at the 2' position of the benzene moiety can intramolecularly attack the 9 position of the xanthene moiety to form a spirocycle, resulting in loss of both absorption and fluorescence. Regulation of this intramolecular spirocyclization has been utilized for the development of various fluorescence probes, as exemplified in reports from several groups, including ours[24–28]. The strength of this molecular design is that the activation ratio of the signal can theoretically be almost infinite. We decided to adopt this strategy to develop pH-activatable probes, because we expected that the benzene moiety above the xanthene moiety (see Fig. 1a for the definition) could be freely modified without affecting activation of the probes (see discussion section for details), so that it should be easy to add a modification site for conjugation of the probes to biomolecules. We have reported that 2-hydroxymethyl tetramethylrhodamine (HMTMR; called 2-HM OR (oxygen-rhodamine) in this paper) pH-dependently forms a spirocycle (Fig. 1a) with a pK_a of 9.6[25]. (This is the same value as pK_{cycle}, which is defined as the pH value at which the absorbance of the compound decreases to half the maximum absorbance as a result of the intramolecular spirocyclization[24]; to avoid confusion, we use only the term pK_a in this report.) Since far-red to NIR-emitting group-14 rhodamines, such as silicon-rhodamine (SiR) and germanium-rhodamine (GeR), have higher reduction potentials compared to oxygen-rhodamines, we hypothesized that the electrophilicity at the 9 position of the xanthene moiety in these rhodamines bearing a hydroxymethyl group at the 2' position would be higher, thereby shifting the pK_a to the more acidic region (see Supplementary Note 1 for details). Therefore, we set out to develop novel OFF/ON type NIR pH-activatable probes using these rhodamines.

Development of 2-HM IGeR. To verify our hypothesis, we first prepared three derivatives of 2-HM OR, i.e., 2-HM SeR (selenium- rhodamine), 2-HM SiR and 2-HM GeR (Fig. 2a), and examined their photophysical properties and pK_a values (see Supplementary Fig. 1 for the spectra). As expected, the pK_a values of these rhodamines were shifted to a more acidic region as the absorption wavelength becomes longer, and the apparent pK_a of both 2-HM SiR and 2-HM GeR was about 5.7, which is a

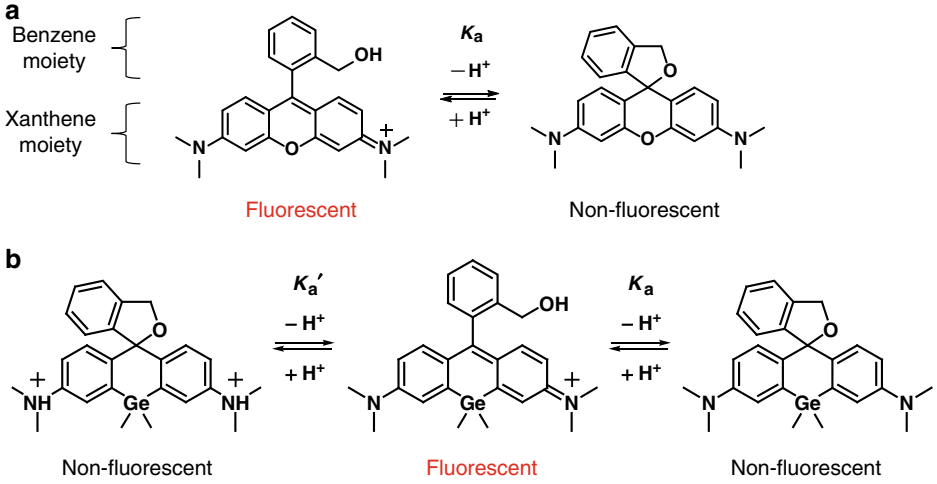

Fig. 1 Equilibrium of open form and spirocyclized form of rhodamine derivatives. Rhodamine derivatives in open form are colored and fluorescent, while those in closed form are colorless and non-fluorescent. **a** Equilibrium of hydroxymethyl tetramethylrhodamine. **b** Proposed equilibrium of hydroxymethyl germanium (Ge)-tetramethylrhodamine

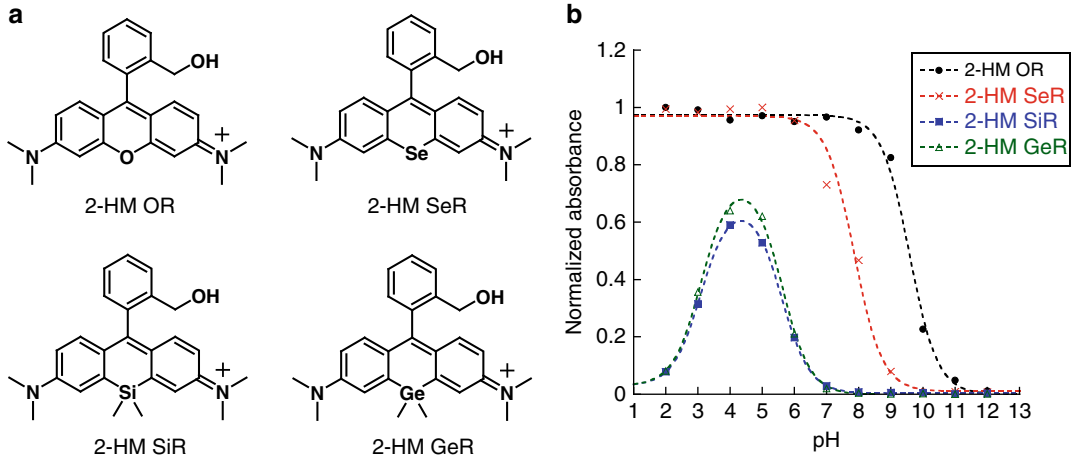

Fig. 2 Properties of 2-hydroxymethyl (HM) rhodamines. **a** Structures of rhodamine derivatives. **b** pH-dependency of absorbance of each probe (1 μM) in 100 mM NaPi buffer. Detection wavelengths were 550 nm for 2-HM OR, 585 nm for 2-HM SeR, 650 nm for 2-HM SiR, and 635 nm for 2-HM GeR

Table 1 Properties of the probes

Dye/dye-protein conjugate	Absorption λ_{max} (nm)	Emission λ_{max} (nm)	Apparent pK_a	Q.E. (Φ_{fl}) of 2-Me analog
2-HM OR	554	572	9.58 ± 0.06	0.35[a]
2-HM SeR	586	604	7.86 ± 0.10	N.D.
2-HM SiR	650	664	5.72 ± 0.08	0.30[a]
2-HM GeR	639	653	5.70 ± 0.03	0.34[a]
2-HM PGeR	646	658	5.44 ± 0.05	0.34[a]
2-HM IGeR	679	693	6.24 ± 0.10	0.25[b]
2-Me GeR	636	651		
Her-GeR	643	656		
Her-HMIGeR	686	700	6.61 ± 0.10	
Her-CypHer	650	665	6.78 ± 0.08	
Avi-GeR	643	656		
Avi-HMIGeR	686	700	5.46 ± 0.08	
Avi-CypHer	651	666	6.86 ± 0.03	

Abs_{max}, Em_{max} (in acidic conditions in which absorbance or fluorescence intensity reach maximum values), apparent pK_a (in 100 mM NaPi buffer), and fluorescence quantum efficiency (Φ_{fl}) of the 2-Me analog of each probe in PBS (pH 7.4) are summarized. For each rhodamine derivative, apparent pK_a values were calculated from the absorbance; see Supplementary Figs. 1 and 2 for values calculated from the fluorescence, which are almost the same. For the probe-Herceptin/avidin conjugates, apparent pK_a values were calculated by fluorescence
[a]Cresyl violet in MeOH (Φ_{fl} = 0.54) as a standard
[b]Cy5.5 in PBS (Φ_{fl} = 0.23) as a standard.

favorable value for detecting intracellular acidic environments (Fig. 2b and Table 1).

However, 2-HM SiR and 2-HM GeR unexpectedly showed different behavior from 2-HM OR and 2-HM SeR, i.e., they also formed a spirocyclized form under strongly acidic conditions (pH < 4) (Figs. 1b and 2b). This can be explained as follows: although the two nitrogen atoms at the 3 and 6 positions of the xanthene moiety are sp^2-hybridized and the dimethylamino groups are in the same plane as the xanthene moiety at neutral pH, a proton coordinates to the amine during the pH change from neutral to acidic, making the electrophilicity of the xanthene moiety of Si-rhodamine or Ge-rhodamine sufficiently high for attack by the hydroxymethyl group to occur, thereby producing a spirocyclized form with two sp^3-hybridized nitrogens in quaternary ammonium salts (Fig. 1b) (In case of O-rhodamine and Se-rhodamine, this process does not occur probably because electrophilicity of the xanthene moiety does not become sufficiently high even after the dication is formed, due to the higher LUMO (lowest unoccupied molecular orbital) energy level of the fluorophores[29]).

Owing to this spirocyclization under acidic conditions, it appears that not all the molecules can be in open form at any pH, since the two acid dissociation constants, pK_a' and pK_a, are proximate (Fig. 1b). To check this, we examined the ratio of the open form by ^{1}H-NMR (Nuclear Magnetic Resonance) measurement, and found that the ratios of the open form of 2-HM SiR and 2-HM GeR at pH 4, where the ratios have the highest values, were 59% and 64%, respectively. This indicates that these rhodamines cannot be fully effective as fluorescence probes, and further, this shortcoming could potentially cause misunderstanding of targeted biological processes.

To overcome this problem, we decided to modify 2-HM GeR, which has a higher fluorescence quantum yield (Φ_{fl}) and a higher rate of the fluorescent ring-opened form in acidic solution, as compared with 2-HM SiR. In general, amines are protonated to form the quaternary ammonium cation under acidic conditions, but cyclic amines are relatively difficult to protonate because of their restricted structural flexibility, resulting in a pK_a shift to the acidic region[1]. Therefore, we hypothesized that if the dimethylamino groups of 2-HM GeR were replaced with cyclic amino groups, spirocyclization in the acidic region would be restricted. Thus, we synthesized 2-HM PGeR and 2-HM IGeR bearing cyclic amino groups at the 3 and 6 positions of the xanthene moiety instead of the dimethylamino groups (Fig. 3a). These cyclic amines were chosen on the basis of a report that these substitutions can change the electrophilicity of benzhydrylium ion[30], which led us expect that they would be useful for fine-tuning the pK_a of the probes for biological applications. Next, we examined the photophysical properties and pH profiles of 2-HM PGeR and 2-HM IGeR, together with 2-Me GeR (Fig. 3, Table 1, and Supplementary Fig. 2), which cannot form a spirocyclized form under acidic conditions due to the lack of a nucleophilic functional group at the 2' position of the xanthene moiety. Although 2-Me GeR showed a pH-independent fluorescence profile, the fluorescence of 2-HM PGeR and 2-HM IGeR showed pH-dependency, and as expected, spirocyclization did not occur under strongly acidic conditions, even at pH 2 (Fig. 3b). The pK_a values of 2-HM PGeR and 2-HM IGeR were around 5.4 and 6.2, respectively (Fig. 3b and Table 1), suggesting that the pK_a values of these probes can indeed be modulated by changing the structure of the substituents at the 3 and 6 positions of the xanthene moiety. The pK_a of 2-HM IGeR (pK_a: 6.2) is

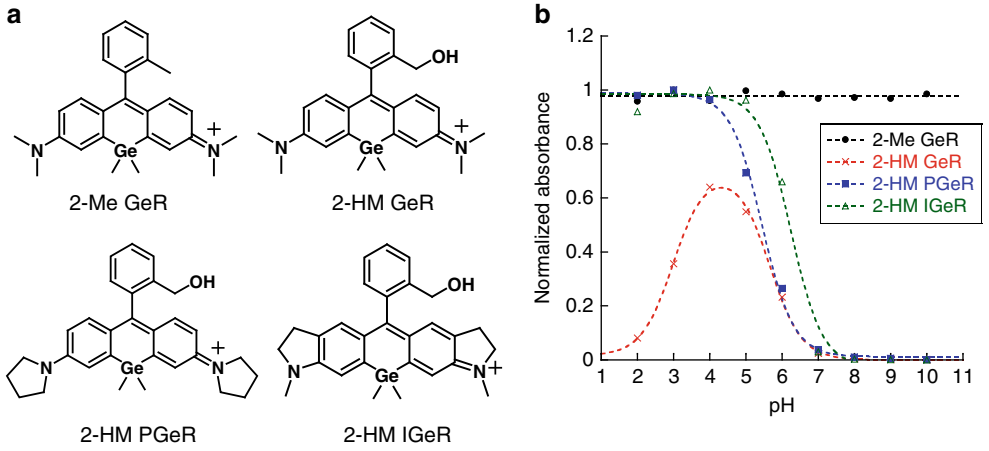

Fig. 3 Properties of Ge-rhodamine derivatives. **a** Structures of optimized pH probes based on Ge-rhodamine. **b** pH-dependency of absorbance of each probe. Detection wavelengths were 635 nm for 2-Me GeR and 2-HM GeR, 645 nm for 2-HM PGeR, and 680 nm for 2-HM IGeR

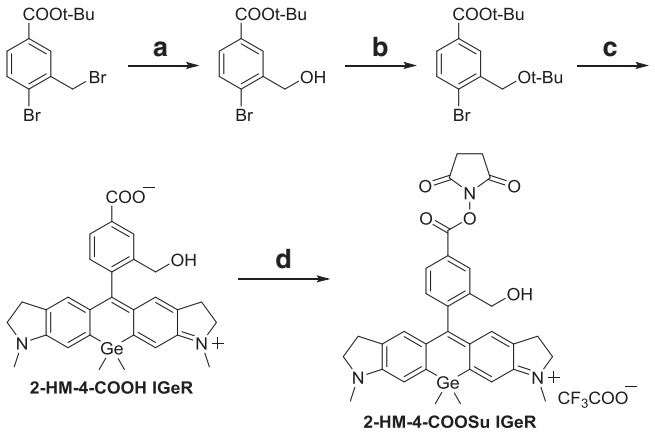

Fig. 4 Synthetic scheme of a near-infrared-emitting pH probe conjugatable to proteins. Reagents: **a** Ag_2SO_4/1,4-dioxane, H_2O, reflux, y. 51%; **b** *t*-BuOH, H_2SO_4, Mg_2SO_4/CH_2Cl_2, r.t., y. 51%; **c** (i) *s*-BuLi/THF, − 78 °C, (ii) IGe-xanthone/THF, − 78 °C to r.t., (iii) 2 N HCl, r.t., (iv) TFA, r.t., y. 52%; **d** NHS, WSCD/DMF, r.t., y. 48%

appropriate for fluorescence imaging of intracellular acidic regions. Further, it is noteworthy that this modification also led to improvement of the absorption and emission wavelengths of the probe as an NIR fluorescence probe (Abs_{max}/Em_{max} = 679/693 nm, about 30 nm longer than 2-HM GeR). The quantum efficiency of this probe was also sufficiently high for biological applications (Table 1).

Conjugation of the pH probe to biomolecules. Next, in order to examine the suitability of this probe for biological applications, we set out to conjugate 2-HM IGeR to biomolecules. For conjugation, we first introduced a succinimidyl ester to obtain 2-HM-4-COOSu IGeR (Figs. 5a and 4). As shown in Fig. 4, we first synthesized *tert*-butyl 3-*tert*-butoxymethyl-4-bromobenzoate, whose carboxy and hydroxyl groups are each protected by a *tert*-butyl group. Then, we lithiated the compound by adding *sec*-butyl lithium, and reacted it with IGe-xanthone. Similarly, we prepared pH-insensitive 2-Me-4-COOSu GeR (Fig. 5a). Then, in order to investigate the pH-dependency of the fluorescence of these labeling reagents when bound to biomolecules, we prepared six conjugates, Her-GeR, Her-HMIGeR, Her-CypHer, Avi-GeR, Avi-HMIGeR, and Avi-CypHer by using 2-Me-4-COOSu GeR, 2-HM-4-COOSu IGeR, or the commercially available NIR pH probe CypHer5E^{TM} mono NHS ester to label Herceptin® or avidin. As expected, Her-GeR and Avi-GeR showed pH-independent fluorescence, while the other compounds showed pH-dependent fluorescence (Fig. 5b, Table 1, and Supplementary Fig. 3). The pK_a values of Her-HMIGeR and Avi-HMIGeR were around 6.6 and 5.5, respectively, which would afford higher activation ratios in the intracellular acidic environment than the relatively neutral pK_a values, around 6.8 and 6.9, of Her-CypHer and Avi-CypHer (Table 1). These results show that it is possible to conjugate 2-HM-IGeR to biomolecules with retention of appropriate pH sensitivity, and further demonstrate that these pH sensors are compatible with structural modification of the benzene moiety to add new functionality: in this case, the ability to conjugate to biomolecules.

Fluorescence imaging of the process of endocytosis. Next, we investigated fluorescence imaging of endocytosis with Her-HMIGeR prepared above. We loaded 150 nM of the conjugate into NIR3T3/HER2(+) cells[5], which are mouse fibroblast cells overexpressing HER2. No fluorescence was observed immediately after addition of Her-HMIGeR to the medium (Fig. 6a), but strong fluorescence appeared as dots in the intracellular region within 24 h (Fig. 6b). This strongly fluorescent region overlapped with lysotracker, and was blocked by addition of Herceptin as a competitive inhibitor (Fig. 6c). This result indicates that Her-HMIGeR was internalized by endocytosis through HER2 and then became fluorescent upon entering acidic lysosomes. On the other hand, when we used Her-GeR, fluorescence was seen even at 0 h (Fig. 6d), and it was difficult to distinguish the fluorescence of the cell membrane from that of lysosomes even at 24 h after incubation with the dye, because Her-GeR is "always on" (Fig. 6e) (in Fig. 6f, Herceptin was again added as a competitive inhibitor to confirm the signal is from the probe binding to HER2). Thus, 2-HM-IGeR conjugated to biomolecules is useful for visualizing the process of endocytosis and the subsequent pH change in the vesicles, whereas Her-GeR is not. We next compared Her-HMIGeR and Her-CypHer. These two probes both showed fluorescence activation upon endocytosis, but there was a marked difference of photostability between them (Fig. 7). When we observed endocytosed Her-HMIGeR or Her-CypHer in living cells by fluorescence confocal microscopy with continuous excitation, we found that almost all the molecules of Her-CypHer were photobleached within 1 min, while Her-HMIGeR showed only slight photobleaching (Fig. 7). Thus, our pH probe-biomolecule conjugate is significantly superior to the

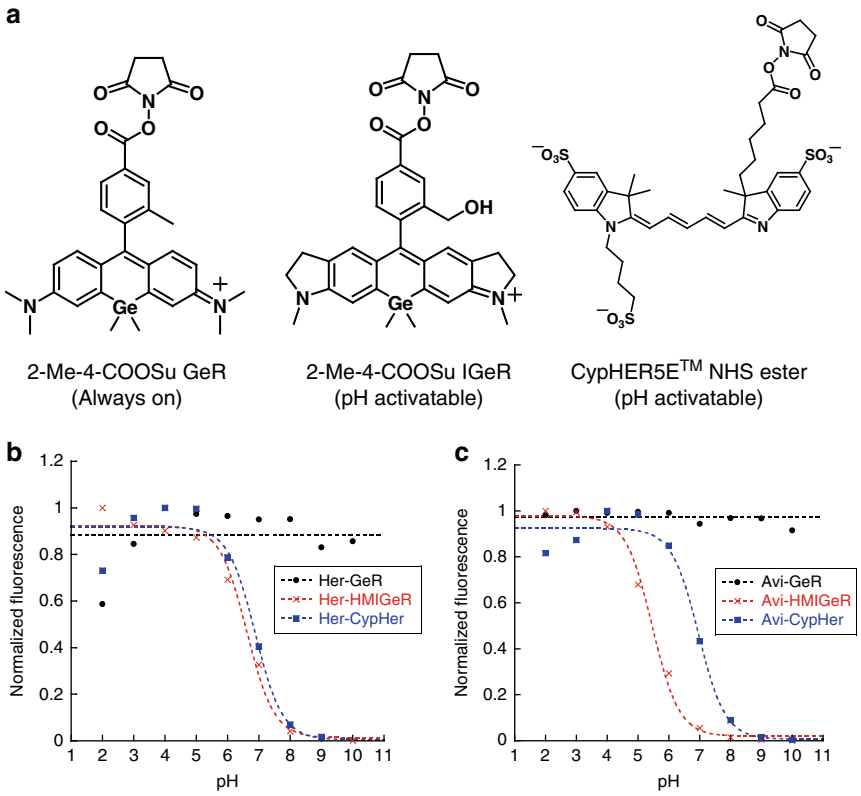

Fig. 5 pH profiles of NIR-emitting pH probe-conjugated Herceptin® and avidin. **a** Structures of biomolecule-conjugatable NIR-emitting pH probes. **b**, **c** pH-dependent fluorescence changes of 0.43 μM Her-GeR, Her-HMIGeR, Her-CypHer (**b**) and Avi-GeR, Avi-HMIGeR, Avi-CypHer (**c**) measured in 100 mM NaPi buffer. Excitation and detection wavelengths were 630 nm and 655 nm for Her-GeR and Avi-GeR, 660 nm and 695 nm for Her-HMIGeR and Avi-HMIGeR, and 630 nm and 665 nm for Her-CypHer and Avi-CypHer, respectively

commercially available cyanine-based conjugate in terms of resistance to photobleaching.

Cancer imaging in a mouse model using probe-labeled avidin. Finally, in order to further investigate the applicability of the probe-biomolecule conjugate for in vivo imaging, we conducted tumor imaging in a mouse model. It has been reported that avidin is recognized by lectins expressed on some types of cancer cells, and is endocytosed[31], thus enabling cancer imaging by using avidin[32–34]. Here, we prepared a peritoneal dissemination model of SHIN3[35] tumors in BALB/c nude mice, and injected Avi-HMIGeR into the peritoneal cavity. After 4 h, the mice were sacrificed and imaging was conducted similarly to the reported method[26,36]. We could clearly visualize disseminated cancers (Fig. 8). This result indicates the usefulness of our probe-biomolecule conjugate for cancer imaging as well.

Discussion

For biological applications, OFF/ON type NIR pH-activatable probes should generally have the following features: (1) an appropriate pK_a to monitor physiological pH changes (pK_a around 6 is suitable to monitor the pH range of 5–7.4); (2) a large fold change of fluorescence intensity between acidic and basic conditions (across the pK_a); (3) ability to be conjugated to biomolecules without impairment of the photophysical properties. Regarding the first point, for example, the pK_a value of the commercially available NIR pH-activatable fluorescence probe CypHer5E™ is 7.3 (according to the product specification sheet of the product, PA15401, GE Healthcare), which is somewhat higher than is desirable to monitor the intracellular acidic region[1–4]. To monitor physiological pH change with high sensitivity, a pK_a of around 6 would be better, as mentioned above, but rational adjustment of the pK_a of cyanine-based probes is difficult. On the other hand, a design based on photoinduced electron transfer (PeT) can provide precise control of pK_a, as shown in our previous study[5], but it is difficult to achieve a large fold fluorescence change with NIR fluorescence probes activated by PeT, because of their low excitation energy[19]. In this context, we have previously reported that Si- or Ge-rhodamines are superior to cyanines in terms of the controllability of fluorescence by PeT because of their higher reduction potential, and we have used them to develop novel pH probes that provide a high fold activation[29]. However, it is not easy to modify these kinds of PeT-based Si- or Ge-rhodamine probes in a way that allows them to be conjugated to biomolecules without alteration of their photophysical properties, because the structure of the benzene moiety above the xanthene moiety is already highly optimized to precisely regulate the PeT phenomenon. Therefore, we required a different design strategy for NIR pH-activatable probes that would meet all three of the above requirements.

Here, we have successfully developed new Ge-rhodamine-based NIR pH-activatable fluorescence probes suitable for biological applications based on control of intramolecular spirocyclization. In particular, we were able to block the undesirable intramolecular spirocyclization under strongly acidic conditions. Our design strategy also enables precise control of the pK_a, in addition to affording desirable absorption and emission wavelengths in the NIR window. Further, our probe design allows simple conjugation of the probe to biomolecules with retention of the photophysical properties. The value of the probes synthesized here is exemplified by the use of Her-HMIGeR to visualize

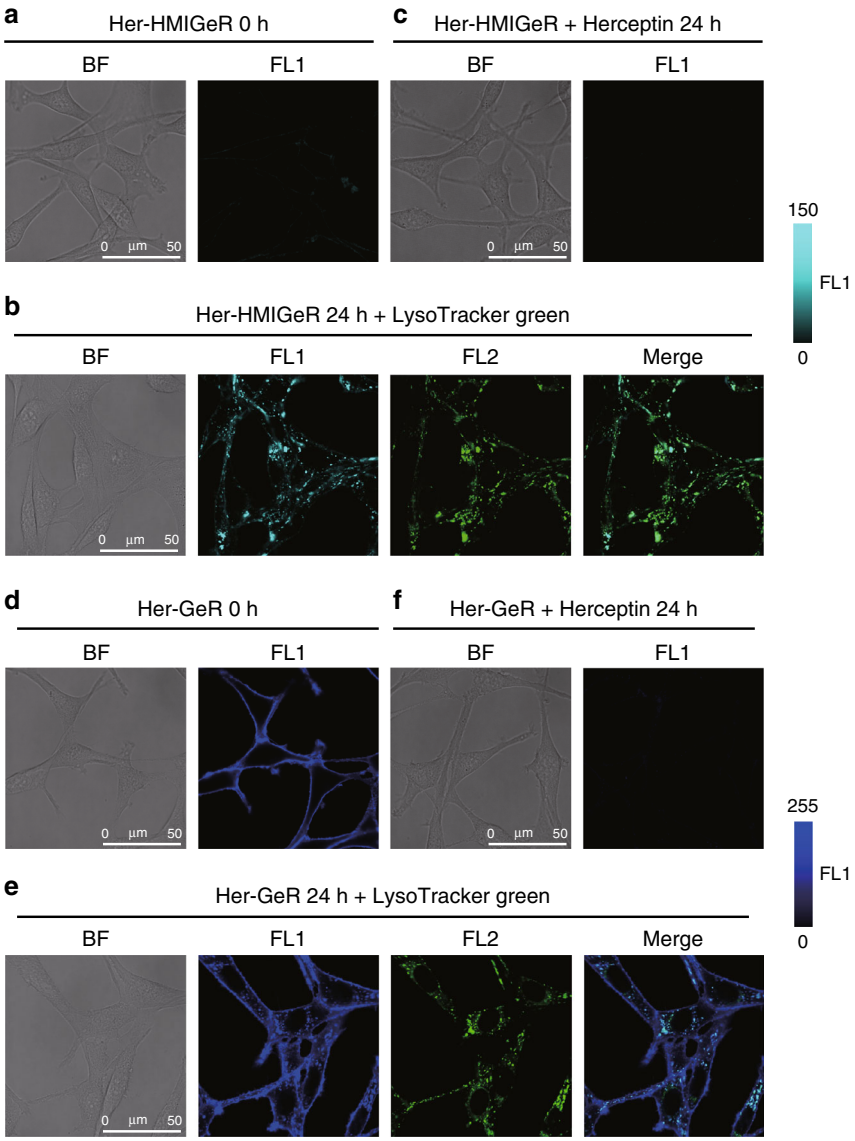

Fig. 6 Visualization of acidic environment during endocytosis in NIH3T3/HER2(+) cells. **a**–**c** Imaging with Her-HMIGeR. **d**–**f** Imaging with Her-GeR. Bright-field and fluorescence images were captured just after 150 nM probe-Herceptin conjugate was loaded into NIH3T3/HER2(+) cells (**a**, **d**). Twenty four hours later, 1 μM LysoTracker® Green was added, and images were captured again (**b**, **e**). Images of NIH3T3/HER2(+) cells treated with 150 nM probe-Herceptin conjugate and 1.5 μM Herceptin® as a competitive inhibitor for 24 h were also obtained (**c**, **f**). BF: Bright-field image. FL1: Fluorescence image of probe-Herceptin conjugate. FL2: Fluorescence image of LysoTracker® Green. Excitation and detection wavelengths were 670 nm and 690–800 nm for Her-HMIGeR, 650 nm and 670–800 nm for Her-GeR, and 488 nm and 500–535 nm for LysoTracker® Green. Scale bars represent 50 μm

endocytosis in living cells, and Avi-HMIGeR to visualize tumors in a mouse peritoneal dissemination model. These results directly show that the pH-activatable fluorescence probe HMIGeR developed in this study fulfills the three requirements discussed above. This probe also offers the advantages of high-quantum efficiency and resistance to photobleaching.

We believe that HMIGeR is currently among the best-in-class pH-activatable near-infrared probes for use in biological and medical research, especially when a high signal-to-noise ratio in the NIR region is required. This probe should be a powerful tool for analyzing various biological processes or diseases in which pH change plays an important role.

Methods

General methods for synthesis of compounds. General chemicals were of the best grade available, supplied by Tokyo Chemical Industries, Wako Pure Chemical, Aldrich Chemical Co., Alfa Aesar, Dojindo, GE Healthcare and Invitrogen, and were used without further purification. NMR spectra were recorded on a JEOL JNM-LA300 instrument at 300 MHz for ^{1}H-NMR and at 75 MHz for ^{13}C NMR. δ values are given in ppm relative to tetramethylsilane. Mass spectra (MS) were measured with a JEOL JMS-T100LC AccuToF using ESI. high performance liquid chromatography (HPLC) analysis was performed on an Inertsil ODS-3 (4.6 × 250 mm) column (GL Sciences Inc.) using an HPLC system composed of a pump (PU-980, JASCO) and a detector (MD-2015 or FP-2025, JASCO). Preparative HPLC was performed on an Inertsil ODS-3 (10.0 × 250 mm) column (GL Sciences Inc.) using an HPLC system composed of a pump (PU-2080, JASCO) and a detector (MD-2015 or FP-2025, JASCO). Detailed synthetic schemes and methods are provided in Supplementary Methods.

Ultraviolet (UV)–visible (Vis) absorption and fluorescence spectroscopy. UV–visible spectra were obtained on a Shimadzu UV-1650. Fluorescence spectroscopic studies were performed on a Hitachi F4500. The slit width was 2.5 nm for both excitation and emission. The photomultiplier voltage was 700 V. Relative fluorescence quantum efficiencies of 2-Me GeR and 2-Me PGeR were obtained by comparing the area under the emission spectrum of the test sample excited at 600 nm with that of a solution of cresyl violet in MeOH, which has a quantum

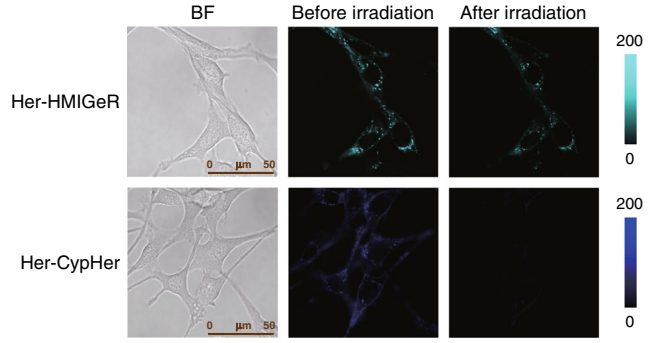

Fig. 7 Photobleaching test to compare photostability of Her-HMIGeR and Her-CypHer. NIH3T3/HER2(+) cells were incubated with 150 nM Her-HMIGeR or Her-CypHer for 24 h, and bright-field and fluorescence images were captured. Then, the cells were exposed to excitation light (with the same power for observation of fluorescence) for 1 min, and fluorescence images were obtained again. Excitation and detection wavelengths were 670 nm and 690–800 nm for Her-HMIGeR, and 650 nm and 670–800 nm for Her-CypHer. Scale bars represent 50 μm

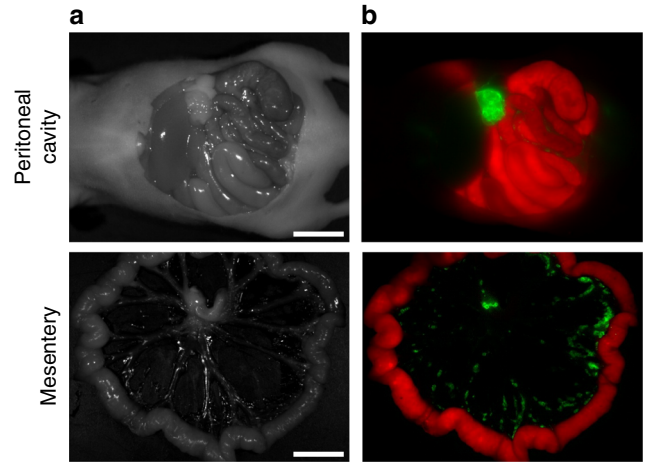

Fig. 8 Fluorescence imaging of peritoneal metastases of SHIN3 cells in a mouse model. The mice were sacrificed at 4 h after peritoneal injection of 100 μg Avi-HMIGeR in 300 μL PBS, and the images were captured after dissection. **a** White light image. **b** Unmixed image. In the unmixed image, fluorescence from the probe and autofluorescence were assigned as green and red, respectively. Ex/Em = 616−661 nm/675 nm LP filter. Scale bars represent 1 cm

efficiency of 0.54[23], and that of 2-Me IGeR was referred to Cy5.5 in phosphate buffered saline (PBS), whose quantum efficiency is 0.23[29].

Calculation of pK_a values. Absorption and fluorescence spectra were measured in 100 mM sodium phosphate buffer at various pH values. The pH profiles of absorbance or fluorescence intensity (at λ_{max}) were fitted to the Henderson–Hasselbalch equation by using KaleidaGraph (Synergy Software) for determination of pK_a values. For 2-HM SiR, 2-HM GeR, and Her/Avi-CypHER, the values at pH 2 and 3 were not used for fitting, because the absorbance and fluorescence were both decreased under these strongly acidic conditions.

Labeling Herceptin® and avidin with the probes. Two equimolar amine-reactive 2-HM-4-COOSu IGeR, 2-Me-4-COOSu GeR, or CypHer5E^{TM} mono NHS ester was reacted with Herceptin® (2.2 mg) or avidin (0.66 mg) in NaPi buffer (1 mL, pH 8.5) for 2 h at r.t. The mixture was purified on a Sephadex G50 column (PD-10, GE Healthcare). Under these conditions, the dye per antibody ratios (D/A) of the prepared conjugates were 0.6 for Avi-CypHer, 0.5 for Her-GeR, Her-CypHer, and Avi-GeR, and 0.3 for Her-HMIGeR and Avi-HMIGeR, as determined from the absorbance of the dyes. (We assumed that ε (molar extinction coefficient) of ring-opened 2-HM GeRs are the same as that of the 2-Me analog ($\varepsilon = 1.0 \times 10^5$ in PBS), and estimated the concentration in acidic solution, which would give almost 100% open form.)

Experiments using living cells. NIH3T3/HER2(+) cells[5] and SHIN3 cells[35] were cultured in Roswell Park Memorial Institute (RPMI) medium supplemented with 10% (v/v) fetal bovine serum, 1% penicillin and 1% streptomycin in a humidified incubator containing 5% CO_2 in air. For fluorescence microscopy, cells were plated on a 35-mm PDL-coated glass-bottomed dish (MatTek Corporation) in the medium.

Endocytosis imaging and photobleaching test. A confocal imaging system (TCS-SP5, Leica) equipped with a white light laser was used. Fluorescence images were taken with simultaneous monitoring of fluorescence at two channels (FL1 = 690–800 nm for Her-HMIGeR or 670–800 nm for Her-GeR and Her-CypHer, FL2 = 500–535 nm). Excitation wavelengths of 670 nm for Her-HMIGeR, 650 nm for Her-GeR and Her-CypHer, and 488 nm for LysoTracker® Green were used. Other conditions, such as the concentrations of probe and antibody and the incubation time, are described in the figure legends.

Tumor imaging with Her-HMIGeR. Six-week-old female BALB/cAJcl-nu/nu mice (CREA Japan, Inc.) were given an intraperitoneal (i.p.) injection of 1×10^6 human ovarian cancer SHIN3 cells suspended in 300 μL PBS. After 10 days, the mice were injected i.p. with freshly prepared Her-HMIGeR (D/A = 0.6) (100 μg in 300 μL PBS), and 4 h later, they were sacrificed by exposure to carbon dioxide. Images were acquired by using a Maestro^{TM} In Vivo Imaging System (CRI Inc., MA, USA), with an excitation filter of 616–661 nm and a 675 nm LP emission filter. The tunable filter was automatically stepped in 10-nm increments from 670 to 900 nm and the camera captured images at each wavelength interval with constant exposure. The fluorescence spectra consisted of intestine autofluorescence and Her-HMIGeR fluorescence, and the two were unmixed based on their spectral patterns with Maestro 2.10.0 software. Experiments involving animals were carried out in accordance with regulations and guidelines for the care and use of experimental animals of the University of Tokyo and approved by the institutional review committees of the the University of Tokyo.

Reporting summary. Further information on research design is available in the Nature Research Reporting Summary linked to this article.

Data availability

All relevant data available is included in this paper and Supplementary Information. All other data are available from the authors upon request.

Received: 24 April 2019 Accepted: 15 July 2019
Published online: 09 August 2019

References

1. Asanuma, D. et al. Acidic-pH-activatable fluorescence probes for visualizing exocytosis dynamics. *Angew. Chem. Int. Ed.* **53**, 6085–6089 (2014).
2. Overly, C. C., Lee, K. D., Berthiaume, E. & Hollenbeck, P. J. Quantitative measurement of intraorganelle pH in the endosomal-lysosomal pathway in neurons by using ratiometric imaging with pyranine. *Proc. Natl Acad. Sci. USA* **92**, 3156–3160 (1995).
3. Cousin, M. A. & Nicholls, D. G. Synaptic vesicle recycling in cultured cerebellar granule cells: role of vesicular acidification and refilling. *J. Neurochem.* **69**, 1927–1935 (1997).
4. Ohkuma, S. & Poole, B. Fluorescence probe measurement of the intralysosomal pH in living cells and the perturbation of pH by various agents. *Proc. Natl Acad. Sci. USA* **75**, 3327–3331 (1978).
5. Urano, Y. et al. Selective molecular imaging of viable cancer cells with pH-activatable fluorescence probes. *Nat. Med.* **15**, 104–109 (2009).
6. Kobayashi, H. & Choyke, P. L. Target-cancer-cell-specific activatable fluorescence imaging probes: rational design and in vivo applications. *Acc. Chem. Res.* **44**, 83–90 (2011).
7. Kobayashi, H., Ogawa, M., Alford, R., Choyke, P. L. & Urano, Y. New strategies for fluorescent probe design in medical diagnostic imaging. *Chem. Rev.* **110**, 2620–2640 (2010).
8. Han, J. & Burgess, K. Fluorescent indicators for intracellular pH. *Chem. Rev.* **110**, 2709–2728 (2010).
9. Hou, J. T. et al. Fluorescent bioimaging of pH: from design to applications. *Chem. Soc. Rev.* **46**, 2076–2090 (2017).
10. Yue, Y. K., Huo, F. J., Lee, S., Yin, C. X. & Yoon, J. A review: the trend of progress about pH probes in cell application in recent years. *Analyst* **142**, 30–41 (2017).

11. Weissleder, R. A clearer vision for in vivo imaging. *Nat. Biotechnol.* **19**, 316–317 (2001).
12. Hilderbrand, S. A. & Weissleder, R. Near-infrared fluorescence: application to in vivo molecular imaging. *Curr. Opin. Chem. Biol.* **14**, 71–79 (2010).
13. Frangioni, J. V. In vivo near-infrared fluorescence imaging. *Curr. Opin. Chem. Biol.* **7**, 626–634 (2003).
14. Egawa, T. et al. Development of a far-red to near-infrared fluorescence probe for calcium ion and its application to multicolor neuronal imaging. *J. Am. Chem. Soc.* **133**, 14157–14159 (2011).
15. Wrobel, A. T., Johnstone, T. C., Deliz Liang, A., Lippard, S. J. & Rivera-Fuentes, P. A fast and selective near-infrared fluorescent sensor for multicolor imaging of biological nitroxyl (HNO). *J. Am. Chem. Soc.* **136**, 4697–4705 (2014).
16. Shcherbakova, D. M. & Verkhusha, V. V. Near-infrared fluorescent proteins for multicolor in vivo imaging. *Nat. Methods* **10**, 751–754 (2013).
17. Lee, H. et al. Near-infrared pH-activatable fluorescent probes for imaging primary and metastatic breast tumors. *Bioconjugate Chem.* **22**, 777–784 (2011).
18. Myochin, T. et al. Rational design of ratiometric near-infrared fluorescent pH probes with various pKa values, based on aminocyanine. *J. Am. Chem. Soc.* **133**, 3401–3409 (2011).
19. Cooper, M. E. G., Adie, S., Kalinka, E. & pH-Sensitive, S. Cyanine dyes for biological applications. *J. Fluor.* **12**, 425–429 (2002).
20. Hilderbrand, S. A. & Weissleder, R. Optimized pH-responsive cyanine fluorochromes for detection of acidic environments. *Chem. Commun.* **14**, 2747–2749 (2007).
21. Kiyose, K. et al. Molecular design strategies for near-infrared ratiometric fluorescent probes based on the unique spectral properties of aminocyanines. *Chem. Eur. J.* **15**, 9191–9200 (2009).
22. Zhang, Z. & Achilefu, S. Design, synthesis and evaluation of near-infrared fluorescent pH indicators in a physiologically relevant range. *Chem. Commun.* **47**, 5887–5889 (2005).
23. Takahashi, S. et al. Development of a series of practical fluorescent chemical tools to measure pH values in living samples. *J. Am. Chem. Soc.* **140**, 5925–5933 (2018).
24. Kamiya, M. et al. beta-Galactosidase fluorescence probe with improved cellular accumulation based on a spirocyclized rhodol scaffold. *J. Am. Chem. Soc.* **133**, 12960–12963 (2011).
25. Kenmoku, S., Urano, Y., Kojima, H. & Nagano, T. Development of a highly specific rhodamine-based fluorescence probe for hypochlorous acid and its application to real-time imaging of phagocytosis. *J. Am. Chem. Soc.* **129**, 7313–7318 (2007).
26. Urano, Y. et al. Rapid cancer detection by topically spraying a gamma-glutamyltranspeptidase-activated fluorescent probe. *Sci. Transl. Med.* **3**, 110ra119 (2011).
27. Sakabe, M. et al. Rational design of highly sensitive fluorescence probes for protease and glycosidase based on precisely controlled spirocyclization. *J. Am. Chem. Soc.* **135**, 409–414 (2013).
28. Koide, Y., Urano, Y., Hanaoka, K., Terai, T. & Nagano, T. Development of an Si-rhodamine-based far-red to near-infrared fluorescence probe selective for hypochlorous acid and its applications for biological imaging. *J. Am. Chem. Soc.* **133**, 5680–5682 (2011).
29. Koide, Y., Urano, Y., Hanaoka, K., Terai, T. & Nagano, T. Evolution of group 14 rhodamines as platforms for near-infrared fluorescence probes utilizing photoinduced electron transfer. *ACS Chem. Biol.* **6**, 600–608 (2011).
30. Baidya, M. & Mayr, H. Nucleophilicities and carbon basicities of DBU and DBN. *Chem. Commun.* **15**, 1792–1794 (2008).
31. Yao, Z. et al. The relationship of glycosylation and isoelectric point with tumor accumulation of avidin. *J. Nucl. Med.* **40**, 479–483 (1999).
32. Yao, Z. et al. Avidin targeting of intraperitoneal tumor xenografts. *J. Natl. Cancer Inst.* **90**, 25–29 (1998).
33. Mamede, M. et al. Hepatocyte targeting of 111In-labeled oligo-DNA with avidin or avidin-dendrimer complex. *J. Control. Release* **95**, 133–141 (2004).
34. Sato, N. et al. Tumor targeting and imaging of intraperitoneal tumors by use of antisense oligo-DNA complexed with dendrimers and/or avidin in mice. *Clin. Cancer Res.* **7**, 3606–3612 (2001).
35. Imai, S., Kiyozuka, Y., Maeda, H., Noda, T. & Hosick, H. L. Establishment and characterization of a human ovarian serous cystadenocarcinoma cell line that produces the tumor markers CA-125 and tissue polypeptide antigen. *Oncology* **47**, 177–184 (1990).
36. McCann, T. E. et al. Activatable optical imaging with a silica-rhodamine based near infrared (SiR700) fluorophore: a comparison with cyanine based dyes. *Bioconjugate Chem.* **22**, 2531–2538 (2011).

Acknowledgements

We thank Dr. Tasuku Ueno and Dr. Mako Kamiya for their generous advice. This research was supported in part by a Grant-in-Aid for JSPS Fellows (to Y.K., R.K., and K.N.), by The Mochida Memorial Foundation for Medical and Pharmaceutical Research (grant to R.K.), and by a Grant-in-Aid for Scientific Research (KAKENHI) (Grant Nos. 23249004 and 26111012 to Y.U., Specially Promoted Research Grant Nos. 22000006 to T. N., and Grant Nos. 16H05099, 18H04609, and 19H05414 to K.H.) from the Ministry of Education, Culture, Sports, Science and Technology of Japan, and SENTAN, JST to K.H.

Author contributions

Y.K. conducted most of the experiments. Y.K., R.K., K.H. and Y.U. analyzed the results. K.N. contributed to synthesis of the compounds. R.K., K.H. and Y.U. wrote the manuscript. T.K., T.N. and H.K. contributed to project discussions and edited the manuscript. Y.U. supervised the entire project.

Additional information

Supplementary information accompanies this paper at https://doi.org/10.1038/s42004-019-0194-4.

Competing interests: The authors declare no competing interests.

Reprints and permission information is available online at http://npg.nature.com/reprintsandpermissions/

Publisher's note: Springer Nature remains neutral with regard to jurisdictional claims in published maps and institutional affiliations.